

Geophysical Research Letters

RESEARCH LETTER

10.1029/2020GL087256

Key Points:

- Unusual observation of EPB with smaller scale irregularities appears initially at top and dilatory development in narrow funnel region later
- We suggest that rapid vertical rise of bubble due to large background electric field surpassed the rate of cascading secondary instabilities
- Hypothesis is tested with the available background ionospheric conditions and high-resolution bubble model simulations

Supporting Information:

- Supporting Information S1
- Movie S1
- Movie S2

Correspondence to:

S. Tulasi Ram,
tulasi@iigs.iigm.res.in

Citation:

Tulasi Ram, S., Ajith, K. K., Yokoyama, T., Yamamoto, M., Hozumi, K., Shiokawa, K., et al. (2020). Dilatory and downward development of 3-m scale irregularities in the funnel-like region of a rapidly rising equatorial plasma bubble. *Geophysical Research Letters*, 47, e2020GL087256. <https://doi.org/10.1029/2020GL087256>

Received 27 JAN 2020

Accepted 30 MAY 2020

Accepted article online 9 JUN 2020

Dilatory and Downward Development of 3-m Scale Irregularities in the Funnel-Like Region of a Rapidly Rising Equatorial Plasma Bubble

S. Tulasi Ram¹ , K. K. Ajith² , T. Yokoyama³ , M. Yamamoto³ , K. Hozumi⁴ , K. Shiokawa⁵ , Y. Otsuka⁵ , and G. Li²

¹Indian Institute of Geomagnetism, Navi Mumbai, India, ²Institute of Geology and Geophysics Chinese Academy of Sciences, Beijing, China, ³Research Institute for Sustainable Humanosphere, Kyoto University, Uji, Japan, ⁴National Institute of Information and Communications Technology, Koganei, Japan, ⁵Institute for Sun-Earth Environmental Research, Nagoya University, Nagoya, Japan

Abstract The equatorial plasma bubbles, once developed, grow nonlinearly into topside ionosphere, and simultaneous secondary instabilities lead to the development of shorter scale irregularities. The altitudinal growth and generation of smaller scale irregularities determine the spatio-temporal occurrence and the intensity of ionospheric scintillations at wide spectrum of radio waves and have significant implications on the GNSS/Satellite Based Augmentation Systems. In this letter, we present a unique equatorial plasma bubble observation from equatorial atmosphere radar that provides hitherto undisclosed evidence for the smaller (3-m) scale irregularities initially developing at higher altitudes and subsequently developing to lower altitudes in a narrow funnel-like structure. The responsible mechanisms for early development of shorter scale irregularities in the topside and their subsequent development at lower altitudes are discussed in light of difference between the time scales of altitudinal growth and cascading rate of secondary instabilities through high-resolution bubble model simulations.

1. Introduction

The turbulent plasma density irregularities in the night time ionosphere, known as equatorial plasma bubbles (EPBs), are one of the important concerns for the trans-ionospheric radio communications and satellite-based augmentation systems. The steep vertical density gradient owing to quick recombination of bottomside plasma after sunset and the rapid uplift of equatorial *F*-layer due to prereversal enhancement in the equatorial zonal electric field makes the postsunset hours as the most conducive period for the development of EPBs (Farley et al., 1986; Fejer et al., 1999; Tulasi Ram et al., 2006). Further, the zonal large-scale wave structure (LSWS) in the bottomside ionosphere provides the necessary seed to trigger the Rayleigh-Taylor instability for the onset of EPB (Ajith et al., 2015; Tsunoda, 2005; Tsunoda et al., 2018; Tsunoda & White, 1981; Tulasi Ram et al., 2012, 2014). The EPBs generally grow from the “crest” or “upwelling” of the LSWS under the action of polarization electric fields developed within them. The EPB then quickly grow into nonlinear phase where the successive cascading of secondary instabilities leads to the development of a wide spectrum of irregularities with scale sizes ranging from few hundred kilometers to few centimeters (Haerendel, 1973; Huba et al., 1985; Ossakow et al., 1979; Tsunoda, 1985; Yokoyama et al., 2014). As the EPBs grow altitudinally into the topside ionosphere, they elongate along the equipotential magnetic field lines to low latitudes affecting the trans-ionospheric communications at equatorial and low-latitude regions over a wide band of radio frequencies. Several earlier reports have clearly demonstrated the magnetic field line elongation of plasma bubbles (Tsunoda, 1980) and simultaneous appearance of symmetric bubbles at magnetically conjugate locations using both observations (Otsuka et al., 2002; Fukushima et al., 2015) and model simulations (Yokoyama et al., 2014).

The altitudinal growth of an EPB and the cascading rate of secondary instabilities are influenced by several factors such as base height of the *F*-layer, ion-neutral collision frequency, ratio of *F*- to *E*-region field-line-integrated conductivities, strength of polarization electric fields, and the density gradient at the walls of depletion (Keskinen et al., 2003; Ossakow et al., 1979). As the bubble grows into topside, the significant reduction of ion-neutral collisions and increased ratio of *F*- to *E*-region field-line-integrated conductivities

give rise to more rapid development of intermediate-to-shorter scale irregularities at topside compared lower altitudes (below F -peak) (Bhattacharyya, 2004; Huba et al., 1985). Though observations are sparse, the high-resolution model simulations often show the early development of more turbulent shorter scale structures in the topside ionosphere compared to lower altitudes (e.g., Figures 2 and 3 of Yokoyama et al., 2014; Figure 6 of Tulasi Ram et al., 2017). The important implications of larger population of intermediate-scale irregularities in the topside ionosphere on the L-band scintillations have been recently brought to light by Bhattacharyya et al. (2017). The more turbulent structures in the topside ionosphere map to the low latitudes away from the equator along the equipotential field lines. The greater structuring of EPBs in the topside ionosphere is found to be one of the important factors for the much stronger L-band scintillations at low latitudes and equatorial ionization anomaly crest locations compared to equatorial latitudes (Bhattacharyya et al., 2014 and Bhattacharyya et al., 2017) besides the higher background density and larger density gradients (Bhattacharyya et al., 2003; Groves et al., 1997; Mullen et al., 1985). Hence, it is very important to study the altitudinal development of smaller scale turbulent structures, particularly in view of prediction of L-band scintillations at low latitudes away from the equator.

However, apart from the model simulations, no direct observations have been reported for the early (delayed) development of shorter scale irregularities in the topside (lower altitudes) probably due to the limitations of the experiments. In this paper, we present an unusual observation of EPB with shorter (3-m) scale irregularities that are initially detected at higher altitudes and subsequently developed to lower altitudes, using equatorial atmosphere radar (EAR) at Kototabang, Indonesia. The responsible mechanisms for this unique observation have been discussed in terms of rapid altitudinal growth of large-scale EPB to the topside ionosphere due to strong background electric fields and subsequent development of smaller scale irregularities.

2. Data

The 16-beam coherent backscatter observations from the 47 MHz EAR at Kototabang (0.2° S geog.lat, 100.32° E geog.long and 9.92° S dip latitude), Indonesia, have been considered to investigate the temporal and spatial evolution of a rare EPB occurred during the postsunset hours of 10 November 2011. The frequency modulated continuous wave ionosonde observations from a low-latitude station, Chiang Mai (18.76° N, 98.93° E and 12.7° N dip latitude), have been considered to study the virtual height variations of background F -layer over this sector. Further, the in situ ion $E \times B$ drift velocity data from the ion velocity meter (IVM) on board the C/NOFS (Communication/Navigation Outage Forecasting System) satellite have been considered in this study.

3. Results

Figure 1 shows the altitude-time-intensity (Figure 1a) and altitude-time-Doppler velocity (Figure 1b) maps of field-aligned irregularities (FAIs) observed from the EAR during the postsunset hours of 10 November 2011. The green and red curves in Figures 1a and 1b represent the sunset terminators corresponding to the local and apex altitudes, respectively. Of the particular interest in this study is the EPB that developed just few minutes after apex sunset (around 1945 to 2000 LT) over the EAR location. This EPB exhibits strong Bragg scatter echoes at topside (above 450 km), and a narrow tail-like structure of faint echoes extended downward (Figure 1a). Similar tail-like structures below the plasma bubbles are sometimes can be observed from EAR (e.g., Fukao et al., 2004; Patra et al., 2005) during the postsunset hours. Interestingly, the Doppler velocity in this narrow tail-like structure exhibits very high values reaching nearly -150 m/s indicating the strong upward flow in this region (Figure 1b).

With a view to further examine the spatial and temporal evolution of this EPB, the fan-sector maps constructed using multibeam (16-beams) observations of EAR are presented at 2-min intervals from 1942 to 2004 LT in Figure 2. The values of Y axis on the left-hand and right-hand sides indicate the altitudes over EAR location and the corresponding apex location, respectively. The green and red curves in the panels of Figure 2 indicate the local and apex sunset terminators, respectively. The thin dashed lines in the fan sector maps represent the projections of 16 individual beams. The cardinal directions with respect to radar field of view are indicated in each frame. It can be observed from this figure that faint backscatter echoes of 3-m scale FAI initially appeared near the top-edge of the radar range around 450–470 km (corresponding to the apex altitudes of $\gtrsim 660$ km) on central and three eastward beams at 1944 LT. The thin contour line

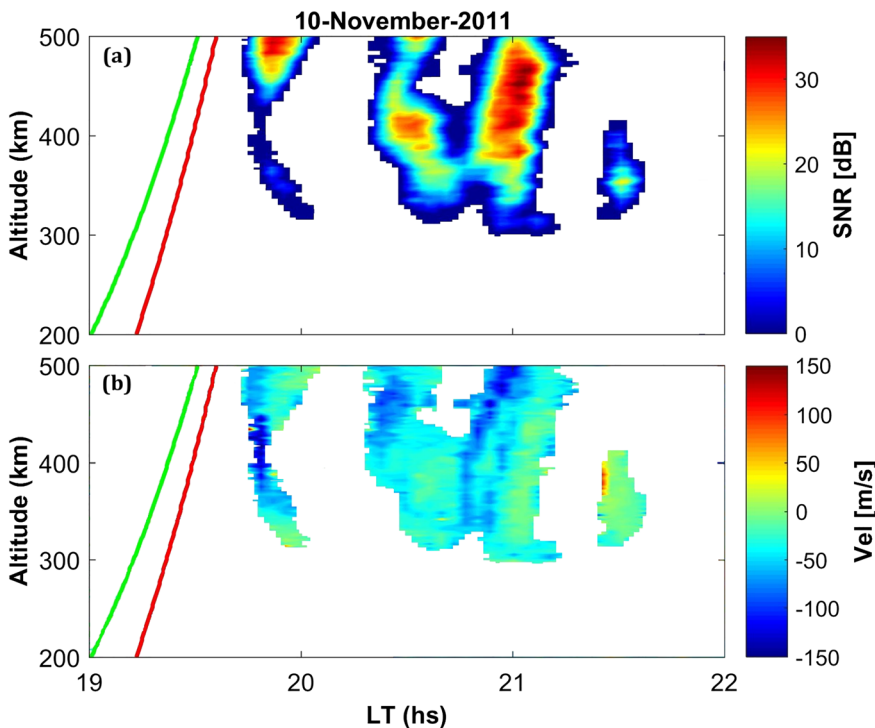


Figure 1. (a) Altitude-local time-intensity and (b) altitude-local time-Doppler velocity maps of *F*-region field-aligned irregularities observed from 47 MHz equatorial atmosphere radar (EAR) at Kototabang on 10 November 2011. The green and red curves in both the panels indicate the local and apex sunset terminators.

encompassing FAI echoes corresponds to the signal-to-noise ratio of -3 dB. The echoes become stronger by 1946 LT, and a very small tail-like structure with faint echo appears on the forth eastward beam from the center. At 1948 LT, the bubble has grown further and the narrow tail-like structure becomes conspicuous near the bottomside of EPB, which progressively becomes stronger and extended downward with time. These observations clearly indicate that the shorter (3-m) scale irregularities are initially detected at topside and later progressively developed at lower altitudes in a narrow band-like structure. Note that the initial detection of echoes (3-m scale irregularities) on the central beams at 1944 LT and their subsequent development below in a narrow funnel-like region is occurred completely within the radar coverage area from 1944 to 2000 LT. This gives the clear, direct, and unambiguous observations of the spatial and temporal evolution of 3-m scale irregularities within the radar coverage area and rules-out the possibility of irregularity development outside the radar coverage and subsequently moving into the radar coverage. These observations, to the best of our knowledge, are the first and convincing observational evidence for the early development of shorter scale irregularities in the topside and their subsequent development at lower altitudes.

4. Discussion

The prereversal enhancement in the zonal electric field during the postsunset hours causes the rapid elevation of equatorial *F*-layer and the growth of bottomside LSWS via interchange instability (Tsunoda et al., 2011, 2018). The EPBs are generally launched from the “crests” or “upwellings” of the LSWS (Tsunoda, 2005; Tsunoda et al., 2018; Tsunoda & White, 1981). Both the observations and the nonlinear plasma bubble models consistently show that the bubble quickly rises to the topside through a narrow funnel-like depletion characterized by strong upward flow of low-density plasma and then bifurcate in to more turbulent structures through cascading secondary instabilities (Huang & Kelley, 1996; Huba et al., 2008; Otsuka et al., 2004; Woodman & LaHoz, 1976; Yokoyama et al., 2014; Zalesak & Ossakow, 1980, and references therein). The narrow tail-like structure at the bottomside of EPB observed in Figures 1 and 2 is characterized by strong upward flow with Doppler velocities of nearly 150 m/s (Figure 1b) indicating that this structure corresponds to the funnel-like region. However, a

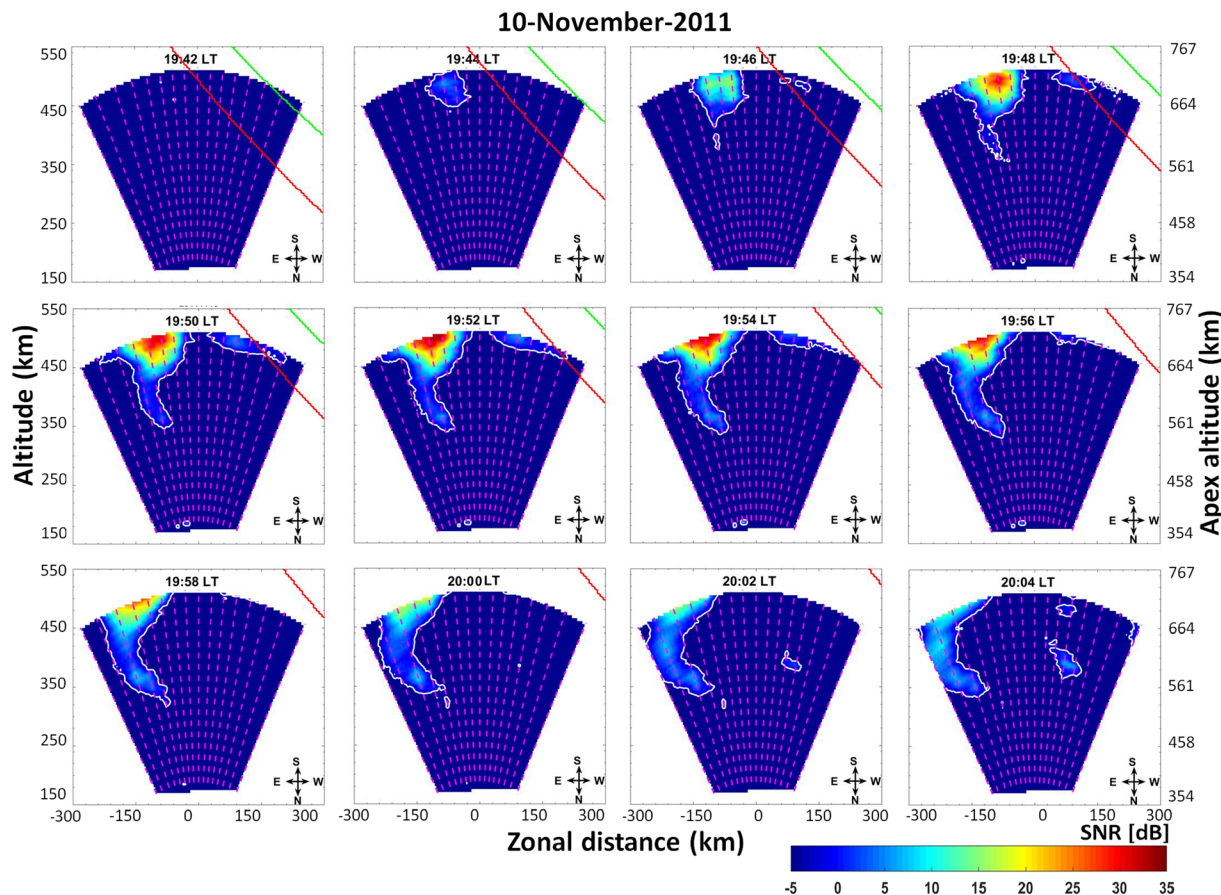


Figure 2. Fan sector maps constructed from the 16-beam observations of equatorial atmosphere radar showing the spatial and temporal evolution of interesting equatorial plasma bubble during the postsunset hours of 10 November 2011. The green and red curves in each frame indicate the local and apex sunset terminators. The thin dashed lines represent the projections of 16 individual beams of equatorial atmosphere radar. The thin contour encompassing the echoes corresponds to signal-to-noise ratio of -3 dB .

careful observation reveals that the FAI (3-m scale irregularities) echoes in this funnel-like region appear a few minutes later compared to the FAI in the topside (Figure 2). The dilatory development of shorter scale irregularities in the funnel-like region could probably due to relative time scales of vertical rise of bubble and the rate of cascading secondary instabilities.

It is shown through observations as well as model simulations that the vertical rise velocity of EPB is significantly controlled by the background zonal electric field (Dao et al., 2016; Tulasi Ram et al., 2017). The larger eastward electric field causes the rapid elevation of the *F*-layer to higher altitudes and in turn increases the growth rate of bubble through reduced ion-neutral collisions. As the large-scale bubble is vertically rising upward, the cascading of secondary instabilities simultaneously setup to produce the different scale sizes of irregularities ranging from larger scale (few hundred kilometers) to intermediate scale (few kilometers) and to shorter scale (few meters to centimeters). Under the very large background electric field conditions, it could be possible that the vertical rise velocity of bubble can be exceedingly high compared to the cascading rate of secondary instabilities and the bubble can quickly surge to the topside ionosphere. Further, the rate of cascading instabilities and the development of shorter scale irregularities are much faster at higher altitudes compared to low altitudes due to reduced ion-neutral collision frequency (Huba et al., 1985), enhanced field-line integrated conductivity ratio between *F* and *E* regions (Bhattacharyya, 2004), and low background plasma densities (Huba & Ossakow, 1979; Otsuka et al., 2004). Hence, the more turbulent shorter scale irregularities would initially develop at higher altitudes and subsequently at lower altitudes including in the funnel-like region as seen in Figures 1 and 2. This dilatory development of smaller scale irregularities in the funnel-like region is not regularly observed from radar observations, probably, due to the simultaneous development of smaller scale irregularities with the rising bubble. However, under the very

large background electric field conditions, the vertical rise velocity of the bubble can be slightly faster compared to the cascading rate of secondary instabilities making the delayed appearance of 3-m scale irregularities at lower altitudes visible from the radar observations (Figures 1 and 2).

Unfortunately, we do not have the observations of background electric field and *F*-layer height on this date due to nonoperation of equatorial ionosonde over this region to validate the above hypothesis. However, the ionosonde observations from the nearby low-latitude station, Chiang Mai (CMU), around the same longitude sector exhibit a rapid uplift of *F*-layer indicating the presence of strong background eastward electric field conditions. Figure 3a shows the variation of *F*-layer virtual height ($h'F$) at CMU (red curve) during the postsunset hours of 10 November 2011. The $h'F$ variations on the other quiet days in the month of November 2011 are also shown in the figure as gray dots and their monthly averaged curve in blue color with error bars. One can observe that the $h'F$ at CMU on this day (red curve) deviates significantly from its monthly mean curve (blue) and exhibits a sharp uplift from 298 to 344 km during ~1915 to 1945 LT corresponding to an upward drift velocity of 25.55 m/s. Following this rapid uplift, intense spread-*F* echoes have been observed at CMU between 1945 and 2,130 LT as indicated by cyan line in Figure 3a. It should be noted that the prereversal enhancement in the background electric field is mainly centered on the equator and gradually tapered down as moving away from the equator. Considering this fact, an upward drift of 25.51 m/s at CMU is very high at 12.7° dip latitude and one would expect a much rapid uplift of *F*-layer at equatorial latitudes. Since we do not have observations over equatorial latitudes on this day, we tried to estimate a rough statistical relationship on the postsunset peak upward drift between CMU and an equatorial station Chumphon (CPN, 10.72°N, 99.37°E and 3.0° dip latitude) over the same longitude sector based on the simultaneous observations during November 2013 and November 2014 (similar solar activity periods). It is found that the postsunset peak upward drift at the equatorial station CPN is nearly double that of low-latitude station CMU (not shown in figure). Though a very coarse estimation, it suggests that the upward drift at the equator could be nearly 50 m/s indicating a strong background electric field of ~1.8 mV/m.

Figure 3b shows the longitudinal variation of in situ $E \times B$ drift measured from the IVM onboard the C/NOFS satellite orbiting around ~785 km altitude around the same time. The ground tracks of C/NOFS orbit on this day (pink curve) along with the locations of EAR (KTB) and Ionosonde (CMU) are shown in the inset of Figure 3b. The C/NOFS in situ $E \times B$ drift at southern low latitudes also exhibits a strong upward drift of ~25–20 m/s over this (95–100°E) longitude during the postsunset hours. It may be noted that the C/NOFS observations are farther away from the equator (nearly 18°S dip latitude) and at a very high altitude (~785 km). Therefore, the observations from CMU ionosonde and C/NOFS consistently indicate that the large background electric fields must be prevailing during the postsunset hours of 10 November 2011 over the equatorial region in this longitudinal sector. The large background electric field helped to the rapid vertical rise of large-scale bubble in to topside, and the 3-m scale irregularities initially developed at higher altitudes. In other words, the vertical rise velocity of the large-scale bubble surpassed the cascading rate of secondary instabilities at lower altitudes leading to the dilatory development of shorter scale irregularities in the funnel-like region.

In order to further test this hypothesis, the high-resolution plasma bubble (HIRB) model (Yokoyama et al., 2014) simulations are carried out under two different values of background electric fields. This model solves the continuity and momentum equations for O^+ (*F* region) and NO^+ (*E* region) in the magnetic dipole coordinate system (refer Yokoyama et al., 2014, for more details on the model description). The present model simulations are carried out at 1-km spatial resolution in the three dimensions. Figure 4 presents the altitudinal development of EPBs in the equatorial plane under the background zonal electric fields of $E = 0.5$ mV/m (case-1; Figures 4a and 4b) and $E = 2$ mV/m (case-2; Figures 4c and 4d). The top panels show the bubble phase when the initial smaller scale irregularities are started to develop. The bottom panels show the bubble under its fully developed phase. The time elapsed for the corresponding phases of EPBs are indicated in each panel for the both cases. The movies showing the temporal and spatial evolution of EPBs at every 100-s intervals for both cases are provided as supporting information (S1 and S2). It can be seen from Figure 4 that the EPB structure is raised to an altitude of ~500 km at 2000 s and ~700 km at 2800 s for the case-1 ($E = 0.5$ mV/m; left panels). On the other hand, for case-2 ($E = 2$ mV/m; right panels), the EPB structure is raised to nearly the same altitudes within half of the time taken for case-1. This clearly indicates the much faster vertical rise of EPB under higher background electric fields. Further, the smaller scale structures

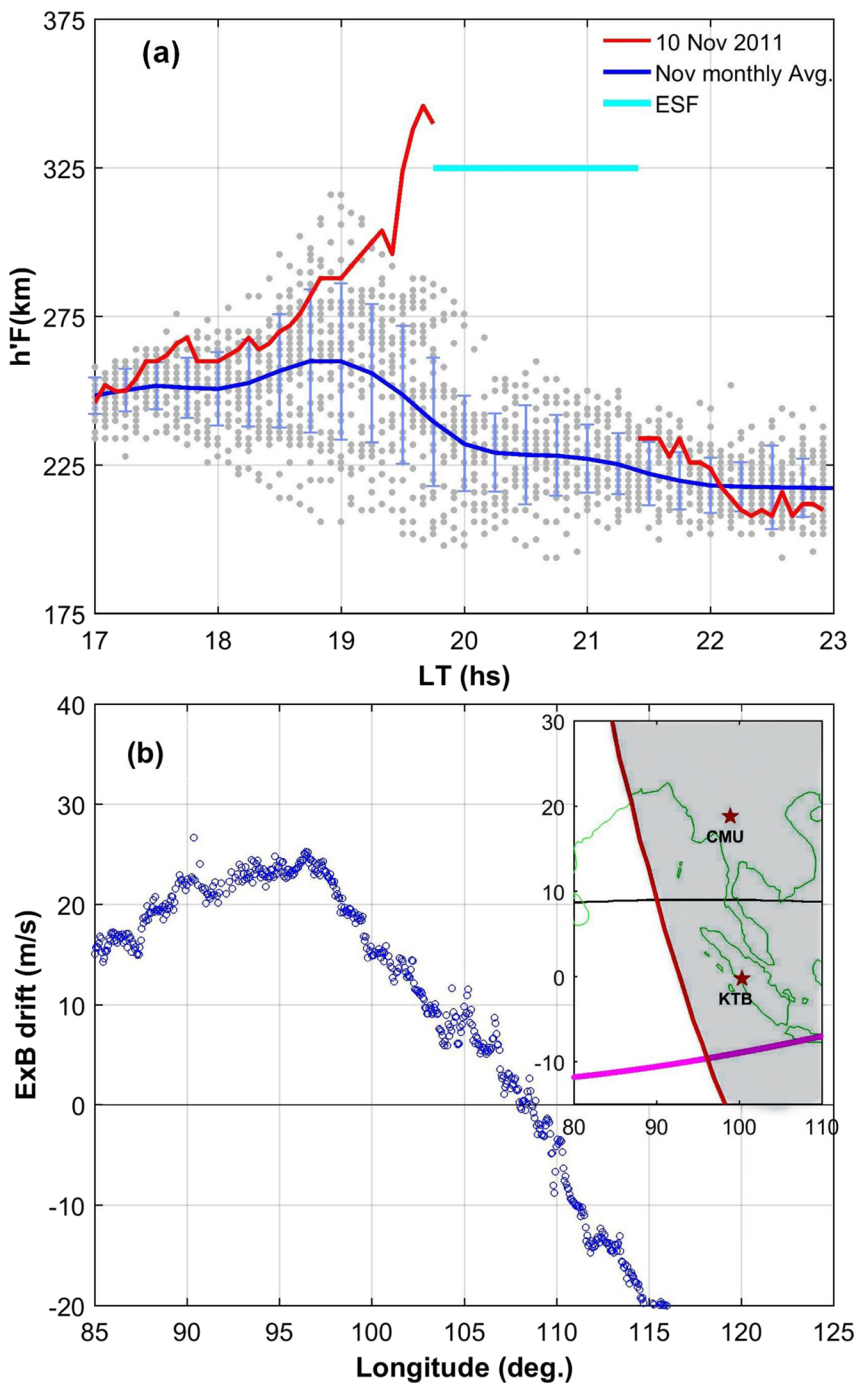


Figure 3. (a) Local time variation of F -layer virtual height ($h'F$) at a low-latitude station Chiang Mai (CMU; red curve) along with the monthly mean variation (blue curve with error bars). The gray dots represent the $h'F$ observations during the quiet days of November 2011. The cyan horizontal bar indicates the occurrence of spread- F . (b) Longitudinal variation of in situ $E \times B$ drift velocity of ions measured from ion velocity meter onboard the C/NOFS satellite. The inset shows the ground track of C/NOFS (pink curve), geomagnetic equator (black curve), and the locations of CMU and KTB along with the sunset terminator (red curve).

initially develop at the topside of the bubble without any significant smaller scale structures in the funnel region as indicated in the figure (top panels). When the bubble is fully developed and rose to a top altitude of 700 km (bottom panels), one can see the more populated smaller scale turbulent structures in the funnel region for case-1 (enclosed by red box Figure 4b); however, no significant smaller structures

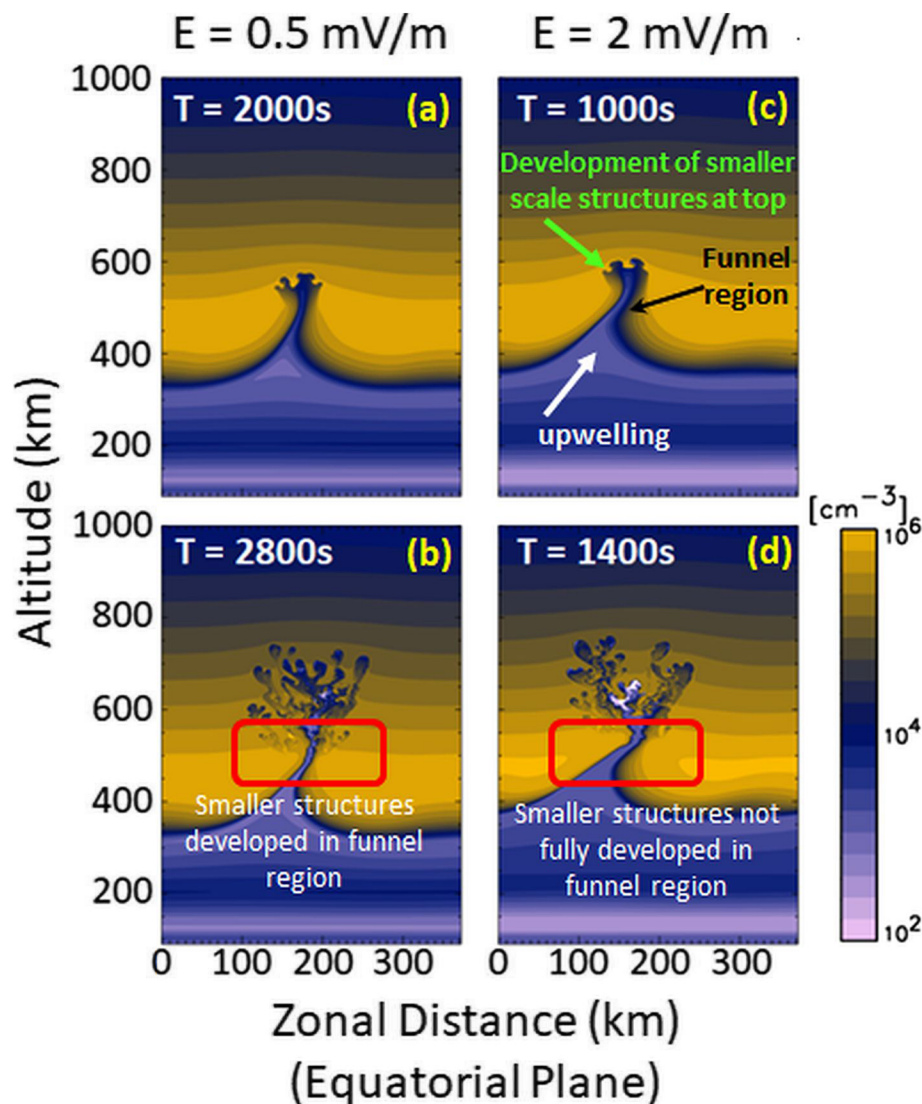


Figure 4. Spatial and temporal evolution of equatorial plasma bubble and shorter scale structures using high-resolution bubble model simulations under two background electric field (E) conditions set to 0.5 mV/m (a and b) and 2 mV/m (c and d). Refer text for more details.

are seen in the funnel region for case-2 (Figure 4d). That means, under normal background electric field conditions, when the EPB is growing progressively upward, the simultaneous cascading of secondary instabilities leads to the development of smaller scale irregularities. This is what happens during most of the cases, and by the time the bubble rises to the higher altitudes and map to low latitudes (such as at EAR), the smaller scale irregularities had already been developed via cascading secondary instabilities at lower altitudes as well as in the funnel region. However, under very high background electric fields (such as in case-2), the bubble rapidly surges to higher altitudes in very short time and the smaller irregularities will initially develop at the topside of the bubble without any significant smaller scale structures in the bottomside funnel region. These smaller scale structures at the topside of the bubble map to low latitudes and can be detected by low-latitude radar observations such as EAR initially at high altitudes (Figure 2). When the vertical rise of the bubble surpasses the cascading rate of secondary instabilities, the smaller scale irregularities initially appear at topside of the bubble and subsequently at lower altitudes and funnel region with some delay. This dilatory development of smaller scale structures in the funnel region appears as a downward extension of narrow tail-like structure in Figure 2. Further, the whole F -layer and funnel region must be sufficiently elevated for this type of structure (funnel region with smaller scale

irregularities) to be seen at low-latitude EAR, hence, making it a rare observation. It should also be mentioned here that the present HIRB simulations are made with a minimum spatial resolution of 1 km (correspond to intermediate scale irregularities), which is much higher than the 3-m scale irregularities sensitive to the EAR. However, we can expect that the same process can be applicable for the shorter scale irregularities as well according to the cascading mechanism. Nevertheless, Otsuka et al. (2004) have clearly shown that the regions of airglow depletion and 3-m scale FAI irregularities from EAR are spatially well correlated indicating the cascading of irregularities from larger scale to shorter scales.

5. Conclusions

A unique observational evidence for the development of shorter (3-m) scale irregularities initially at the top of a rapidly rising EPB and their subsequent dilatory development at lower altitudes in a narrow funnel-like region had been presented in this paper. The large background electric fields lead to the rapid vertical rise of plasma bubble to the topside where the cascading rate of secondary instabilities is much faster compared to lower altitudes. As a result, the shorter (3-m) scale irregularities are initially developed at the top and subsequently developed at lower altitudes in a narrow funnel-like region. This hypothesis is further validated with the HIRB model simulations, which can resolve the irregularity scale sizes up to 1 km. According to the cascading mechanism of irregularities from larger scale to intermediate scale and to shorter scale, one can assume the early development the shorter (3-m) scale irregularities also at higher altitudes. The rapid vertical growth and more population of turbulent shorter scale irregularities at topside altitudes would have important implications on SBAS (Satellite Based Augmentation Systems) systems and cause much stronger L-band scintillations at low latitudes away from the equator and equatorial ionization anomaly crest latitudes as demonstrated by Bhattacharyya et al. (2017).

Acknowledgments

This work is supported by Department of Science and Technology, Government of India. This work is also partly supported by ISEE, Nagoya University under ISEE international research program (2019-2020). The work of K. Shiokawa is supported by JSPS KAKENHI (15H05815 and 16H06286). The part of this work was also supported by JSPS KAKENHI (16K17814). The simulation work was supported by “Computational Joint Research Program (Collaborative Research Project on Computer Science with High-Performance Computing)” at the Institute for Space-Earth Environmental Research, Nagoya University, Japan. S. T. thanks Archana Bhattacharyya for very helpful discussion. The numerical code used for the simulation requires high-performance computers and is not prepared for publicly accessible servers. The simulation results used in this study are available at the following repository: <https://doi.org/10.5281/zenodo.3614137>. The EAR data can be obtained from <http://www.rish.kyoto-u.ac.jp/ear/index-e.html>. The CMU ionosonde data are available under SEALION network at <http://seg-web.nict.go.jp/sealion/>. The C/NOFS CINDI-IVM data are available at NASA-SPDF (https://spdf.gsfc.nasa.gov/pub/data/cnofs/cindi/ivm_500ms_hdf/).

References

- Ajith, K. K., Ram, S. T., Yamamoto, M., Yokoyama, T., Gowtam, V. S., Otsuka, Y., et al. (2015). Explicit characteristics of evolutionary-type plasma bubbles observed from equatorial atmosphere radar during the low to moderate solar activity years 2010–2012. *Journal of Geophysical Research: Space Physics*, 120, 1371–1382. <https://doi.org/10.1002/2014JA020878>
- Bhattacharyya, A. (2004). Role of E region conductivity in the development of equatorial ionospheric plasma bubbles. *Geophysical Research Letters*, 31, L06806. <https://doi.org/10.1029/2003GL018960>
- Bhattacharyya, A., Groves, K. M., Basu, S., Kuenzler, H., Valladares, C. E., & Sheehan, R. (2003). L-band scintillation activity and space-time structure of low-latitude UHF scintillations. *Radio Science*, 38(1), 1004. <https://doi.org/10.1029/2002RS002711>
- Bhattacharyya, A., Kakad, B., Sripathi, S., Jeeva, K., & Nair, K. U. (2014). Development of intermediate scale structure near the peak of the F region within an equatorial plasma bubble. *Journal of Geophysical Research: Space Physics*, 119, 3066–3076. <https://doi.org/10.1002/2013JA019619>
- Bhattacharyya, A., Kakad, B., Gurram, P., Sripathi, S., & Sunda, S. (2017). Development of intermediate-scale structure at different altitudes within an equatorial plasma bubble: Implications for L-band scintillations. *Journal of Geophysical Research: Space Physics*, 122, 1015–1030. <https://doi.org/10.1002/2016JA023478>
- Dao, T., Otsuka, Y., Shiokawa, K., Tulasi Ram, S., & Yamamoto, M. (2016). Altitude development of postmidnight F region field-aligned irregularities observed using equatorial atmosphere radar in Indonesia. *Geophysical Research Letters*, 43, 1015–1022. <https://doi.org/10.1029/2015GL067432>
- Farley, D. T., Bonelli, E., Fejer, B. G., & Larsen, M. F. (1986). The prereversal enhancement of the zonal electric field in the equatorial ionosphere. *Journal of Geophysical Research*, 91(A12), 13,723–13,728. <https://doi.org/10.1029/JA091A12p13723>
- Fejer, B. G., Scherliess, L., & de Paula, E. R. (1999). Effects of the vertical plasma drift velocity on the generation and evolution of equatorial spread-F. *Journal of Geophysical Research*, 104(A9), 19,859–19,869. <https://doi.org/10.1029/1999JA900271>
- Fukao, S., Ozawa, Y., Yokoyama, T., Yamamoto, M., & Tsunoda, R. T. (2004). First observations of the spatial structure of F region 3-m-scale field-aligned irregularities with the equatorial atmosphere radar in Indonesia. *Journal of Geophysical Research*, 109, A02304. <https://doi.org/10.1029/2003JA010096>
- Fukushima, D., Shiokawa, K., Otsuka, Y., Nishioka, M., Kubota, M., Tsugawa, T., et al. (2015). Geomagnetically conjugate observation of plasma bubbles and thermospheric neutral winds at low latitudes. *Journal of Geophysical Research: Space Physics*, 120, 2222–2231. <https://doi.org/10.1002/2014JA020398>
- Groves, K. M., Basu, S., Weber, E. J., Smitham, M., Kuenzler, H., Valladares, C. E., et al. (1997). Equatorial scintillation and systems support. *Radio Science*, 32(5), 2047–2064. <https://doi.org/10.1029/97RS00836>
- Haerendel, G. (1973). Theory of equatorial spread F, report, Max-Planck Inst. for Phys. and Astrophys, Garching, Germany.
- Huang, C. S., & Kelley, M. C. (1996). Nonlinear evolution of equatorial spread F, 1. On the role of plasma instabilities and spatial resonance associated with gravity wave seeding. *Journal of Geophysical Research*, 101(A1), 283–292. <https://doi.org/10.1029/95JA02211>
- Huba, J. D., Hassam, A. B., Schwartz, I. B., & Keskinen, M. J. (1985). Ionospheric turbulence: Interchange instabilities and chaotic fluid behavior. *Geophysical Research Letters*, 12(1), 65–68. <https://doi.org/10.1029/GL012i001p00065>
- Huba, J. D., Joyce, G., & Krall, J. (2008). Three-dimensional equatorial spread F modeling. *Geophysical Research Letters*, 35, L10102. <https://doi.org/10.1029/2008GL033509>
- Huba, J. D., & Ossakow, S. L. (1979). On the generation of 3-m irregularities during equatorial spread F by low-frequency drift waves. *Journal of Geophysical Research*, 84(A11), 6697–6700. <https://doi.org/10.1029/JA084iA11p06697>
- Keskinen, M. J., Ossakow, S. L., & Fejer, B. G. (2003). Three-dimensional nonlinear evolution of equatorial ionospheric spread-F bubbles. *Geophysical Research Letters*, 30(16), 1855. <https://doi.org/10.1029/2003GL017418>

- Mullen, J. P., Mackenzie, E., Basu, S., & Whitney, H. (1985). UHF/GHz scintillation observed at Ascension Island from 1980 through 1982. *Radio Science*, 20(3), 357–365. <https://doi.org/10.1029/RS020i003p00357>
- Ossakow, S. L., Zalesak, S. T., McDonald, B. E., & Chaturvedi, P. K. (1979). Nonlinear equatorial spread *F*: Dependence on altitude of the *F* peak and bottomside background electron density gradient scale length. *Journal of Geophysical Research*, 84(A1), 17–29. <https://doi.org/10.1029/JA084iA01p00017>
- Otsuka, Y., Shiokawa, K., Ogawa, T., & Wilkinson, P. (2002). Geomagnetic conjugate observations of equatorial airglow depletions. *Geophysical Research Letters*, 29(15), 1753. <https://doi.org/10.1029/2002GL015347>
- Otsuka, Y., Shiokawa, K., Ogawa, T., Yokoyama, T., Yamamoto, M., & Fukao, S. (2004). Spatial relationship of equatorial plasma bubbles and field-aligned irregularities observed with an all-sky airglow imager and the equatorial atmosphere radar. *Geophysical Research Letters*, 31, L20802. <https://doi.org/10.1029/2004GL022086>
- Patra, A. K., Yokoyama, T., Yamamoto, M., Saito, S., Maruyama, T., & Fukao, S. (2005). Disruption of *E* region echoes observed by the EAR during the development phase of equatorial spread *F*: A manifestation of electrostatic field coupling. *Geophysical Research Letters*, 32, L17104. <https://doi.org/10.1029/2005GL022868>
- Tsunoda, R. T. (1980). Magnetic-field-aligned characteristics of plasma bubbles in the nighttime equatorial ionosphere. *Journal of Atmospheric and Terrestrial Physics*, 42(8), 743–752. [https://doi.org/10.1016/0021-9169\(80\)90057-4](https://doi.org/10.1016/0021-9169(80)90057-4)
- Tsunoda, R. T. (1985). Control of the seasonal and longitudinal occurrence of equatorial scintillations by the longitudinal gradient in integrated *E* region Pedersen conductivity. *Journal of Geophysical Research*, 90(A1), 447–456. <https://doi.org/10.1029/JA090iA01p00447>
- Tsunoda, R. T. (2005). On the enigma of day-to-day variability in equatorial spread *F*. *Geophysical Research Letters*, 32, L08103. <https://doi.org/10.1029/2005GL022512>
- Tsunoda, R. T., Saito, S., & Nguyen, T. T. (2018). Post-sunset rise of equatorial *F* layer - or upwelling growth? *Progress in Earth and Planetary Science*, 5(1), 22. <https://doi.org/10.1186/s40645-018-0179-4>
- Tsunoda, R. T., & White, B. R. (1981). On the generation and growth of equatorial backscatter plumes: 1. Wave structure in the bottomside *F* layer. *Journal of Geophysical Research*, 86(A5), 3610–3616. <https://doi.org/10.1029/JA086iA05p03610>
- Tsunoda, R. T., Yamamoto, M., Tsugawa, T., Hoang, T. L., Tulasi Ram, S., Thampi, S. V., et al. (2011). On seeding, large-scale wave structure, equatorial spread *F*, and scintillations over Vietnam. *Geophysical Research Letters*, 38, L20102. <https://doi.org/10.1029/2011GL049173>
- Tulasi Ram, S., Ajith, K. K., Yokoyama, T., Yamamoto, M., & Niranjan, K. (2017). Vertical rise velocity of equatorial plasma bubbles estimated from equatorial atmosphere radar (EAR) observations and HIRB model simulations. *Journal of Geophysical Research: Space Physics*, 122, 6584–6594. <https://doi.org/10.1002/2017JA024260>
- Tulasi Ram, S., Rama Rao, P. V. S., Niranjan, K., Prasad, D. S. V. V. D., Sridharan, R., Devasia, C. V., & Ravindran, S. (2006). The role of post sunset vertical drifts at the equator in predicting the onset of VHF scintillations during high and low sunspot activity years. *Annales de Géophysique*, 24(6), 1609–1616. <https://doi.org/10.5194/angeo-24-1609-2006>
- Tulasi Ram, S., Yamamoto, M., Tsunoda, R. T., Chau, H. D., Hoang, T. L., Damtie, B., et al. (2014). Characteristics of large scale wave structure observed from African and Southeast Asian longitudinal sectors. *Journal of Geophysical Research: Space Physics*, 119, 2288–2297. <https://doi.org/10.1002/2013JA019712>
- Tulasi Ram, S., Yamamoto, M., Tsunoda, R. T., Thampi, S. V., & Gurubaran, S. (2012). On the application of differential phase measurements to study the zonal large scale wave structure (LSWS) in the ionospheric electron content. *Radio Science*, 47, RS2001. <https://doi.org/10.1029/2011RS004870>
- Woodman, R. F., & LaHoz, C. (1976). Radar observations of *F*-region equatorial irregularities. *Journal of Geophysical Research*, 81(31), 5447–5466. <https://doi.org/10.1029/JA081i031p05447>
- Yokoyama, T., Shinagawa, H., & Jin, H. (2014). Nonlinear growth, bifurcation, and pinching of equatorial plasma bubble simulated by three-dimensional high-resolution bubble model. *Journal of Geophysical Research: Space Physics*, 119, 10,474–10,482. <https://doi.org/10.1002/2014JA020708>
- Zalesak, S. T., & Ossakow, S. L. (1980). Nonlinear equatorial spread *F*: Spatially large bubbles resulting from large horizontal scale initial perturbations. *Journal of Geophysical Research*, 85(A5), 2131. <https://doi.org/10.1029/JA085iA05p02131>